Computational Materials Science 138 (2017) 448–461

Contents lists available at ScienceDirect

Computational Materials Science

journal homepage: www.elsevier.com/locate/commatsci

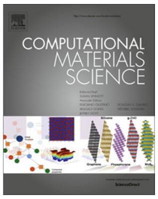

Atomistic to coarse grained simulations of diffusion of small molecules into polymeric matrix

Enqiang Lin [a], Xiaorong You [b], Robert M. Kriegel [b], Ronald D. Moffitt [c], Romesh C. Batra [a],*

[a] Department of Biomedical Engineering and Mechanics, M/C 0219, Virginia Polytechnic Institute and State University, MC 0219, Blacksburg, VA 24061, USA
[b] Global Research, The Coca-Cola Company, 1 Coca-Cola Plaza, Atlanta, GA 30313, USA
[c] Global Engineering, The Coca-Cola Company, 1 Coca-Cola Plaza, Atlanta, GA 30313, USA

ARTICLE INFO

Article history:
Received 28 November 2016
Received in revised form 1 July 2017
Accepted 7 July 2017

Keywords:
Diffusion
Polymer
Molecular dynamics
Coarse grained modeling

ABSTRACT

The diffusion of small molecules into a polymeric matrix often occurs on a wide range of length- and time-scales that are not easily accessible by standard atomistic simulations. It has limited applications of atomistic simulations for evaluating barrier properties of a polymeric film associated with the diffusion of small molecules into the film. Here, we present a multiscale scheme that combines atomistic and coarse-grained (CG) simulations for predicting the diffusion of small molecules into a polymeric film. The atomistic simulations are used to parameterize the CG MARTINI force field and to interpret time scales of the resulting CG models. As a case study, the developed scheme is applied to investigate the diffusion of the Octanal (C8) molecules into a polymeric film composed of four different components. Based on the atomistic simulations, the CG parameters for each polymer component in the film are optimized, and their ability to describe the mixed C8-polymer systems and predict the corresponding dynamic properties are tested. The diffusion results from the CG simulations are validated by analyzing effects of the concentration, the temperature, the water and the polymer components' weight ratio changes. It is shown that the CG simulations are much faster than the atomistic simulations and can describe the diffusion of C8 molecules into the polymeric film. This provides an effective way for studying the diffusion of small molecules into a complex polymeric matrix and evaluate its barrier properties.

1. Introduction

The accurate knowledge of transport properties of small molecules in a polymeric matrix is needed in various technological applications. These properties have been predicted through theoretical, experimental and numerical approaches over the last few decades [1–24].

At the macroscopic (continuum) level, the diffusion of small molecules into a polymer film can often be satisfactorily described by Fick's laws [1]. At the molecular level, the classical free volume theory [2–4], the dual-mode sorption model [5,6] and the activation energy model [7,8] have been used to describe the diffusion of small molecules into polymers. These phenomenological models extend our understanding of the diffusion mechanisms and are useful for correlating the measured diffusivities. However, they lack predictive capability since the model parameters are not directly related to the polymer structures.

Various experimental techniques such as the gravimetric [9], isostatic permeation measurement [10], Fourier transform infrared (FT-IR) spectroscopy [11] and nuclear magnetic resonance (NMR) [12] have been developed to study the transport of small molecules through polymeric films. These techniques are mainly based on the sorption and permeation kinetic determinations, and have greatly expanded our ability to measure a wide range of diffusion rates. However, they are expensive, time consuming and labor intensive. The accurate determination of the diffusion properties also is quite challenging since there is no standard method available for measuring them. Depending upon the test method used, large variations in the measured transport coefficients are found. For example, using different permeation methods, the diffusion coefficient of D-limonene was found to vary between 3.7×10^{-14} m^2 s^{-1} and 17×10^{-14} m^2 s^{-1} (by a factor of 4.6) in high-density polyethylene films, and between 3.7×10^{-16} m^2 s^{-1} and 32×10^{-16} m^2 s^{-1} (by a factor of 8.6) in polypropylene films [13–15].

Atomistic simulations are a powerful research tool for studying the diffusion of small molecules into polymers. They are widely used to characterize the molecular-level structural and dynamics

---

* Corresponding author.
E-mail address: rbatra@vt.edu (R.C. Batra).

http://dx.doi.org/10.1016/j.commatsci.2017.07.011
0927-0256/

details of penetrator-polymer systems that usually are not accessible with experimental techniques, and have been applied to compute the diffusion coefficients of small molecules into various polymer films [16–21]. For example, Karlsson et al. [16] found that the simulated diffusivity and the activation energy of D-limonene in molten polyethylene were within 30% and 16% of their experimental values. They also observed that the penetration of D-limonene molecules occurred via the tumbling process. Wang et al. [17] assessed the diffusion coefficients of 13 small molecules (e.g., limonene, linalool and citral) in amorphous polyethylene terephthalate (PET) using atomistic simulations. Their simulated results were found to be very close to the experimental values, which suggested the effectiveness of the molecular dynamics (MD) method to estimate the diffusion coefficients. Despite the extensive use of atomistic simulations in predicting the diffusion properties, due to their inherent limitations of length and time scales, they can only model the penetrator-polymer systems made of hundreds of thousands of atoms and the corresponding diffusion trajectories are computed from simulation results for a few nanoseconds. Since the normal diffusive regime might still be far away, it has hindered the use of atomistic simulations for assessing more accurate values of the diffusion coefficients and consequently evaluate barrier properties of the polymer film [22]. This limitation has been overcome, at least partially, by adopting the coarse-grained (CG) simulations.

The CG simulations extend the accessible size and time duration by lumping a group of atoms into a pseudo-atom or bead to reduce system's degrees of freedom and by using a larger time step size as a result of the smoother interparticle interactions than those in the MD simulations. Various CG models such as the structure-based [23,24] and the thermodynamics-based [25–28] have been developed for this purpose. Here, we use the thermodynamics-based MARTINI force field developed by Marrink et al. [27,28]. In the MARTINI force field, the interaction parameters are determined by reproducing system's mass density and the free energy partitioning between polar and apolar phases of a number of chemical building blocks. Compared to other CG methods, this parameterization process has made the CG modeling of new molecules relatively easy, and hence suitable for modeling complex polymer matrix systems. Though the MARTINI force field was originally developed for lipid bilayers and subsequently extended to proteins, there are no theoretical impediments for applying it to polymer systems [29].

In this work, we present a multiscale simulation method that combines the atomistic and the MARTINI force field modeling to study the diffusion of small molecules into polymeric films. The atomistic simulations are used to parameterize the MARTINI force field and to calculate the self-diffusion coefficients of the small molecules for interpreting the CG time scales. As a case study, we investigate the diffusion of Octanal (C8) molecules into a polymeric film composed of four different components. The C8-polymer system is selected for its wide application in the food industry where the C8 molecules are usually used as fragrance agents to provide orange-like taste to the product. During storage of these products, the diffusion of C8 molecules into the protective polymeric film lining often occurs, which results in a loss of concentration balance in the food and affects the taste. The rate of C8 diffusion into the polymer film plays an important role in determining the concentration loss rate and hence the shelf life of the food. This work focuses on (i) exploiting a multi-scale scheme to determine the self-diffusion coefficients of C8 molecules and (ii) evaluating the barrier properties of the protective polymer film. Even though the diffusion of only C8 molecules has been investigated, the proposed multiscale simulation scheme can be readily extended to other small molecules (i.e., eugenol and D-limonene) and polymer systems.

The remainder of the paper is organized as follows. In Section 2, we describe the CG force field parameterization and the optimization for the C8-polymer film system. In Section 3, the multiscale approach that combines the atomistic and the CG modeling is used to study the diffusion of C8 molecules into the polymeric film. The performance of the developed CG model at different temperatures and in the presence of water molecules is also discussed. The findings of our work are summarized in Section 4.

2. Development of models for the C8-polymer

2.1. Atomistic models

The preparation of the polymer film model is based on its four components: methyl acrylate, poly(ethylene-co-acrylic acid) (EAA), hydrogen peroxide (H_2O_2) and poly(ethyleneimine) solution 50% (w/v) in H_2O. Their weight percentages are listed in Table 1. In applications, the methyl acrylate and the EAA serve as primary components due to their excellent water barrier properties while H_2O_2 and the poly(ethyleneimine) solution are used as the polymerization initiator and the crosslinking agent to link the two main components to form the final network of the polymer film. Based on the analysis of possible polymerization and curing mechanisms occurring in the mixture of the four components, it is assumed that the final heterogeneous polymer film is mainly made of poly(methyl acrylate) (PMA), EAA, and linear and branched poly(ethyleneimine) (LPEI and BPEI) polymers. Their chemical structures are illustrated in Fig. 1. Due to the complex polymerization process of preparing the film, it is very challenging to construct an atomistic model that accurately describes the connected film system. Thus, in the current study, the simulated film is prepared by directly mixing the four polymers without modeling crosslinking. Based on the weight proportions listed in Table 1, 20 PMA chains with 20 repeating units ($n = 20$), 87 EAA chains with 3 repeating monomers ($n = 3$) of 14 mers ethylene ($x = 14$) and 1 mer acrylic ($y = 1$), 5 LPEI chains with 10 repeating units ($n = 10$) and 5 BPEI chains with only 1 repeating unit ($n = 1$) are chosen to represent the polymer film. By investigating this uncured film, deep insights into the diffusion of small molecules into this polymeric film can still be gained.

2.2. Coarse-grained modeling

The CG modeling of the polymeric film involves two fundamental steps: mapping of atoms into CG beads and the parameterization of the interaction potentials among the CG beads. The choice of atoms to be mapped is often arbitrary in CG modeling. In the MARTINI force field, the original mapping scheme is based on the 4-to-1 rule. That is, on average four heavy atoms (non-hydrogen) are mapped into one CG bead. However, considering the structural symmetries of the four components in the polymer film and to minimize the number of CG bead types, this unified 4-to-1 scheme is not always the best strategy for the current polymer system with four chemical components. Here, the finer rules (e.g., 2-to-1 and 3-to-1) are also applied in modeling the four polymer components, as shown in Fig. 2, with the objective of keeping as many structural characteristics of these polymer chains as possible. For the CG beads interaction potentials, we choose both the structural and the thermodynamic properties as the target properties for the parameterization. Distributions of the distances and the angles from the atomistic simulations are used to parameterize the bonded interactions. The non-bonded interactions are characterized by following conventions in the MARTINI force field to reproduce the mass density and the radius of gyration of the polymer chains from the atomistic simulations.

Table 1
Components and their weight percentages in the polymeric film.

Component	Methyl acrylate	EAA	H_2O_2	Poly(ethyleneimine) solution 50% (w/v) in H_2O
wt%	40	40	15	5

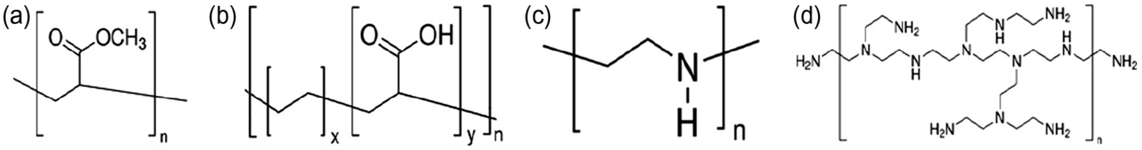

Fig. 1. Chemical structures of (a) PMA; (b) EAA; (c) LPEI and (d) BPEI.

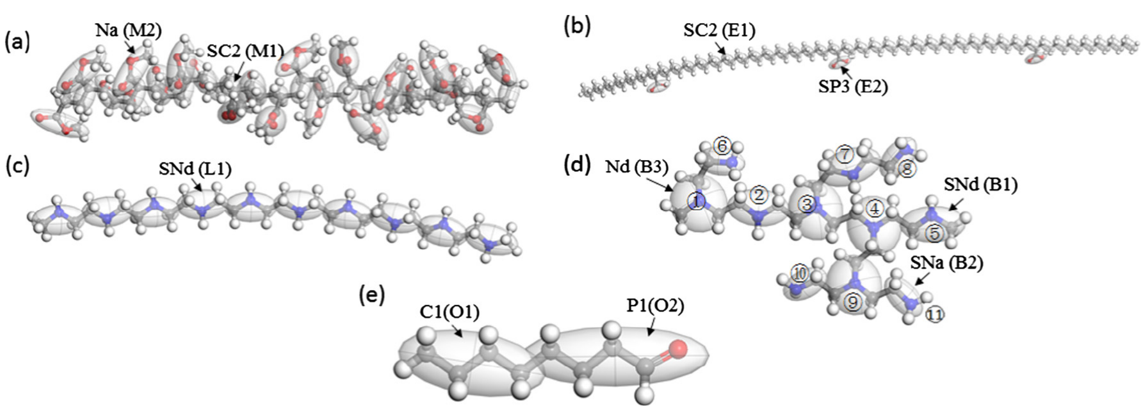

Fig. 2. The atomistic and the coarse-grained descriptions of (a) PMA, (b) EAA, (c) LPEI, (d) BPEI polymers, and (e) C8 molecule. (For interpretation of the references to colour in this figure legend, the reader is referred to the web version of this article.)

2.2.1. Mapping

The finer rules along with the original 4-to-1 mapping scheme in the MARTINI force field are applied in the CG modeling of the four polymer components in the film to better match their chemical structures. As shown in Fig. 2, for the PMA polymer, each methyl acrylate monomer is represented by two MARTINI beads, with the Na bead representing the side methyl-ester group and the SC2 bead for the backbone ethyl parts. For the EAA polymer, the same SC2 bead as that in the PMA polymer is used to describe the backbone ethyl parts, while the side acrylic acid parts are described by the SP3 bead. Unlike the mapping schemes for the EAA and the PMA polymers that are defined on the backbone and the side atoms, the mapping of the BPEI and the LPEI polymers is based on the amino groups. Thus, three kinds of MARTINI beads are used to map the LPEI and the BPEI polymers, with the SNa, the SNd and the Nd beads representing the primary, the secondary and the tertiary amino groups, respectively.

After the CG mapping, the polymer film is described by only 6 types of beads, and the total number of particles in the film system is also significantly reduced from 28,581 in the atomistic model with 20 PMA, 87 EAA, 5 BPEI and 5 LPEI to 4,828 in the CG model. For computational efficiency, two standard masses are generally used for all beads in the MARTINI force field: 72 amu for the typical beads (4-to-1 mapping) and 45 amu for the finer beads (2-to-1 or 3-to-1 mapping). However, in the current study, the assignment of these two standard masses to all beads will significantly underestimate the dynamics and overestimate the mass density of the system. Thus, more realistic masses are employed in the simulations. The masses of the SC2, SP3, Na, SNd, SNa and Nd beads in the film system are set equal to 26, 45, 72, 45, 45 and 56 amu, respectively. For the C8 molecule, the original 4-to-1 rule is applied for the CG mapping. Thus, the C1 and P1 beads with the mass of 72 amu are used to represent the molecule, as shown in Fig. 2e.

2.2.2. Parameterization

Given the above-described CG models (Fig. 2), the success of the MD diffusion simulations depends on the accurate description of the bonded and the non-bonded interactions between the CG beads. In the MARTINI force field, the following harmonic potential functions are used to describe the bonded (bond and angle) interactions:

$$V_{bond}(r) = \frac{1}{2}K_{bond}(r - r_0)^2 \tag{1}$$

$$V_{angle}(\theta) = \frac{1}{2}K_{angle}(\cos(\theta) - \cos(\theta_0))^2 \tag{2}$$

where K_{bond} and K_{angle} are the interaction strengths; θ_0 and r_0 are the equilibrated bond-angle and bond length, respectively. The distance and the angle distributions from the atomistic simulations are used as the target properties to parameterize the bonded interactions. During the parameterization, both the atomistic and the CG systems for each polymer component that contain 40–200 chains are generated and equilibrated at 300 K and 1 atm in the NPT ensemble for 5 ns. Then, the atomistic trajectories are converted into the corresponding CG trajectories by extracting the centers of mass (COMs) positions of groups of atoms, according to the mapping schemes exhibited in Fig. 2. From the converted CG trajectories, the distance and the angle distributions between the COMs are calculated. They are used as the targets to match the distribution results obtained directly from the CG simulations. Examples for the EAA polymer are shown in Fig. 3. It can be seen that the distributions obtained

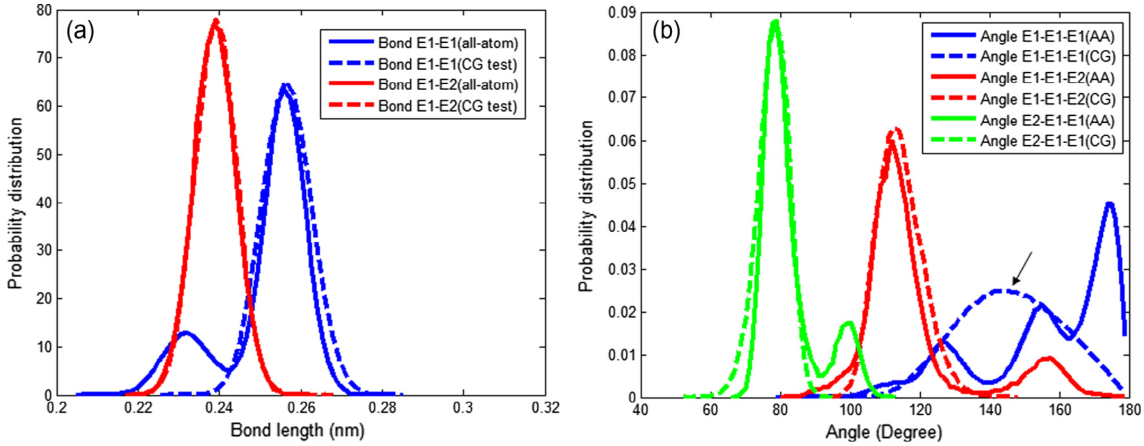

Fig. 3. Probability distributions of (a) bond lengths, and of (b) angles of 40 EAA chains from the atomistic and the CG simulations. The arrow in the figure highlights the E1–E1–E1 CG angle distribution. In this distribution, the strategy to cover as many atomistic angle distribution area as possible is applied due to the multi-modal pattern of the atomistic angle distribution. (For interpretation of the references to colour in this figure legend, the reader is referred to the web version of this article.)

from the CG and the atomistic models match well with each other for the selected values of parameters. Here, it is noted that the atomistic distributions are often bimodal or multimodal due to the atacticity of the polymer chains, while all CG distributions are unimodal because of the harmonic interaction potentials employed in the simulation. Under these situations, to better reflect the averaged properties of the polymer chains, the CG parameters for bonded interactions are adjusted to produce distributions that cover as many atomistic distribution areas as possible (e.g., the E1-E1-E1 angle in Fig. 3). The current CG modeling does not include the torsional terms and only the bond and the angle interactions are treated explicitly for simplicity. The CG torsional distributions of most polymers usually can be well reproduced by using the bond and the angle interactions in combination with suitable non-bonded interactions [28,29]. After these adjustments, the final choice of parameters for the C8-polymer film system is summarized in Table 2. Following the work of Nikunen et al. [30], the chain crossings in CG modeling due to the softer bonded potentials can be prevented when the following topological constraint is satisfied:

$$\sqrt{2}r_{min} > l_{max}$$

Here r_{min} is the radius of each individual CG bead that is impenetrable to other beads, and l_{max} is the maximum stretch for the intramolecular bonds. In the current CG models, r_{min} for each bead is $\geqslant 0.215$ nm (one-half of the minimum value of the van der Waals interaction length 0.43 nm). We checked that for the EAA and the PMA polymers that are the two main ingredients of the polymer matrix, the CG bonded parameters satisfied the uncrossability condition. Even though some of the CG bonded parameters for the BPEI and the LPEI do not satisfy the uncrossability condition, the nonphysical bond crossing between them and the EAA or the PMA chains is avoided due to the repulsive effects from the EAA or the PMA beads. Furthermore, even if the BPEI and the LPEI chains theoretically can cross into each other, their small amounts and well-dispersed distribution in the polymer matrix will prevent the bond crossing from occurring. Thus, we expect that the molecules crossing each other is a rare event and has a negligible effect on the dynamics of the simulated CG systems.

For the non-bonded interactions, the shifted 12-6 Lennard-Jones (L-J) potential is used in the MARTINI force field:

Table 2
CG parameters of bonded interactions for the C8-polymer film system.

Polymer component	Bond	r_0 (nm)	K_b (kJ mol^{-1} nm^{-2})	Angle	θ_0 (°)	K_a (kJ mol^{-1} nm^{-2})
PMA	M1–M1	0.24	12,700	M1–M1–M1	180	4.15
	M1–M2	0.27	21,100	M1–M1–M2	100	4.32
				M2–M1–M1	80	10.83
EAA	E1–E1	0.257	38,500	E1–E1–E1	180	12.50
	E1–E2	0.235	51,300	E1–E1–E2	110	21.705
				E2–E1–E1	75	38.022
LPEI	L1–L1	0.355	2,600	L1–L1–L1	180	9.57
BPEI	B1–B2	0.31	17,100	1–2–3	110	673.57
	B1–B3	0.37	27,100	2–3–4	110	305.38
	B2–B3	0.312	33,800	3–4–5	110	204.96
	B3–B3	0.385	16,300	8–7–3	120	100.78
				6–1–2	40	9.98
				10–9–4	70	8.73
				11–9–4	160	12.50
				10–9–11	40	167.73
				3–4–9	140	100.78
				5–4–9	40	4.55
				2–3–7	120	12.50
				4–3–7	80	16.684
C8	O1–O2	0.47	1,250	–	–	

$$V_{LJ}(r) = 4\varepsilon_{ij}\left[\left(\frac{\sigma_{ij}}{r}\right)^{12} - \left(\frac{\sigma_{ij}}{r}\right)^{6}\right] \quad (3)$$

where σ_{ij} represents the closest distance between CG beads *i* and *j*, and ε_{ij} is the strength of its interactions. Given the CG bead types (see Fig. 2), the non-bonded parameters, σ and ε, can be determined by following conventions of the MARTINI force field. In Table 3 we have summarized the final choice of the non-boned parameters for the C8-polymer film system. These parameters are verified by comparing the CG mass density and the radius of gyration, R_g, of each polymer component at 300 K with those derived from the atomistic simulations. The verification results are listed in Table 4. It can be seen that the chosen values of the MARTINI non-bonded parameters well reproduce the mass density and R_g of the polymers. Our CG model does not explicitly include the long-range electrostatic interactions.

The electrostatic interaction, as a long-range force, plays two roles in the atomistic models: the non-bonded interactions within each molecule and the non-bonded interactions between molecules. For the former, the well-reproduced radius of gyration results of CG models (see Table 4) confirm that the omission of the electrostatic interactions in the CG modeling has negligible effect on determining dimensions of the polymer chains in the system. For the non-bonded interactions between molecules, the omission of the electrostatic interactions results in a smoother non-bonded interaction that reduces the activation energy for the small molecule diffusion into the CG polymer matrix. However, we note that (i) in Fig. 7b the smoother CG non-bonded interactions do not change the two essential diffusion mechanisms (hopping and trapping) in the system that determine the small molecule diffusion coefficients, and (ii) the "short-range" parts of the electrostatic interactions are actually considered during the CG modeling. They are implicitly included in the CG bonded and non-bonded parameters that reproduce the structure and dynamics of the diffusion systems. Therefore, the omission of the electrostatic interactions in the current CG model, as in many other CG models of polymers available in the literature, will not noticeably affect the modeling of small molecules diffusion into the polymer matrix.

2.3. Simulation details

The aforementioned atomistic and CG models (Fig. 2) are used in the proposed multiscale scheme to simulate the diffusion of C8 molecules into the polymer matrix. Both the C8-polymer mixture and the C8-water-polymer layered systems are simulated to test the capability of the proposed scheme for the diffusion modeling. The C8-polymer mixture systems are prepared as follows. First, the initial configurations for both atomistic and CG models are prepared by randomly packing the 20 PMA, 87 EAA, 5 LPEI and 5 BPEI polymer chains and the added C8 molecules in a periodic box to achieve a mass density of about 0.01 g/cm^3. This low value of the mass density is chosen to ensure that the polymer chains and the C8 molecules are well separated. These initial configurations are then equilibrated at a high temperature, T = 450 K, to fully relax the system. Subsequently, the temperature is reduced to 300 K and 7 cycles of NVT and NPT runs are performed to condense system's mass density to that of its equilibrium state at P = 1 atm. Finally, all atomistic and CG simulations are conducted under NVT ensemble for 10–100 ns depending upon the selected time for monitoring the diffusion behaviors of the C8 molecules. The Nose-Hoover thermostat is used to keep the temperature constant with the coupling time set to 0.1 ps. The thus-prepared atomistic and CG C8-polymer systems are shown in Fig. 4.

The diffusion of C8 molecules into the polymer matrix that serves as a protective film in food products usually occurs in an aqueous environment. Thus, the C8-water-polymer layered systems are also simulated to test the robustness of the developed CG models for describing the water effect on the diffusion process. To construct the layered systems, the mixture of 8 PMA, 35 EAA, 2 LPEI and 2 BPEI polymer chains is first compressed into a film by using the rigid walls, as shown in Fig. 5a. Then, based on dimensions of the prepared polymer film, the C8-water layer is prepared by mixing 50 C8 and 4,000 water molecules (TIP3P water model [31] in the atomistic system and P4 water bead in the CG system) and assembled on top of the polymer film (see Fig. 5c). The rigid walls are kept in the prepared layer system to prevent the water molecules from evaporating too far away during the simulations. Their interactions with the C8-water-polymer systems are set to be weak enough to minimize their influence on the diffusion dynamics. The layer models are periodic in the x- and the y-directions while non-periodic in the assembled direction. During the simulations, the prepared layer models are first equilibrated in the NPT ensemble to relax the configuration. Then, they are run in the NVT ensemble to realize the diffusion. Throughout the simulations, the temperature is kept constant at T = 300 K by using the Nose-Hoover thermostat.

During the simulations, for the atomistic models (either mixture or layer system), the OPLS-aa force field [32] is used to describe all the inter- and intra-molecular interactions in the system. The non-bonded interactions (van der Waals and short-range Coulombic interactions) are truncated at a cutoff distance of 10 Å, while the long-range Coulombic interaction is calculated with the PPPM solver [33]. The simulations are performed with a time step of 1 fs for the overall simulation time of about 50 ns. For the CG mixture and layer models, the developed CG parameters (Tables 2 and 3) are used to describe the system. A cutoff distance of 12 Å with a shifted function starting at 9 Å is used to calculate the non-bonded interactions. Since the CG bead sizes and the interaction potentials are, respectively, larger and smoother than those for the atomistic model, a larger time step of 20 fs is used, and the neighbor list is updated every 10 time steps. All these conditions are standard for the MARTINI force field. The atomistic and the CG simulations are performed with the LAMMPS package [34].

Table 3
CG L-J parameters σ (nm) and (ε (kJ mol^{-1})) for the C8-polymer film system.

	SC2	SP3	Na	SNd	SNa	Nd	C1	P1	P4	Wall
SC2	0.43(2.625)	0.43(2.0)	0.47(2.7)	0.43(2.0)	0.43(2.0)	0.47(2.7)	0.47(3.5)	0.47(3.0)	0.47(2.3)	0.47(0.01)
SP3		0.43(3.75)	0.47(4.5)	0.43(3.375)	0.43(3.375)	0.47(4.5)	0.47(2.3)	0.47(4.5)	0.47(5.0)	0.47(0.01)
Na			0.47(4.0)	0.47(4.5)	0.47(4.0)	0.47(4.5)	0.47(2.7)	0.47(4.5)	0.47(4.0)	0.47(0.01)
SNd				0.43(3.0)	0.43(3.375)	0.47(4.0)	0.47(2.7)	0.47(4.5)	0.47(4.0)	0.47(0.01)
SNa					0.43(3.0)	0.47(4.5)	0.47(2.7)	0.47(4.5)	0.47(4.0)	0.47(0.01)
Nd						0.47(4.0)	0.47(2.7)	0.47(4.5)	0.47(4.0)	0.47(0.01)
C1							0.47(3.5)	0.47(2.7)	0.47(2.0)	0.47(0.01)
P1								0.47(4.5)	0.47(4.5)	0.47(0.01)
P4									0.47(5.0)	0.47(0.01)
Wall										0.0(0.0)

Table 4
Atomistic and CG mass density and radius of gyration of the four polymer components at 300 K.

	PMA		EAA		LPEI		BPEI	
	Atomistic	CG	Atomistic	CG	Atomistic	CG	Atomistic	CG
Density (g cm^{-3})	1.148	1.201	0.88	0.876	0.997	0.999	1.009	1.045
Radius of gyration, R_g (nm)	0.887	0.818	1.632	1.638	0.829	0.975	0.566	0.527

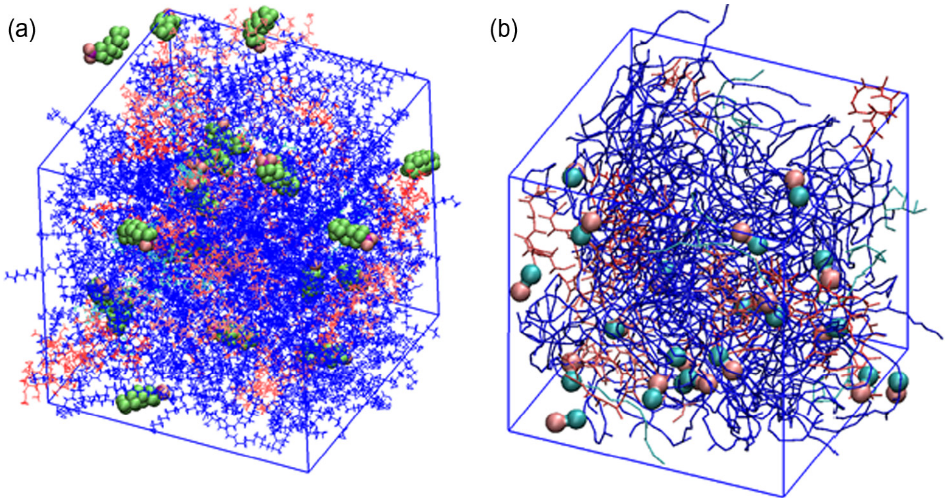

Fig. 4. (a) Atomistic, and (b) CG model of the equilibrated C8-polymer mixture system at 300 K. The red, the blue and the green colors represent, respectively, the PMA chains, the EAA chains, and both the LPEI and the BPEI chains. The C8 molecules are explicitly described by the atoms and the CG beads. (For interpretation of the references to colour in this figure legend, the reader is referred to the web version of this article.)

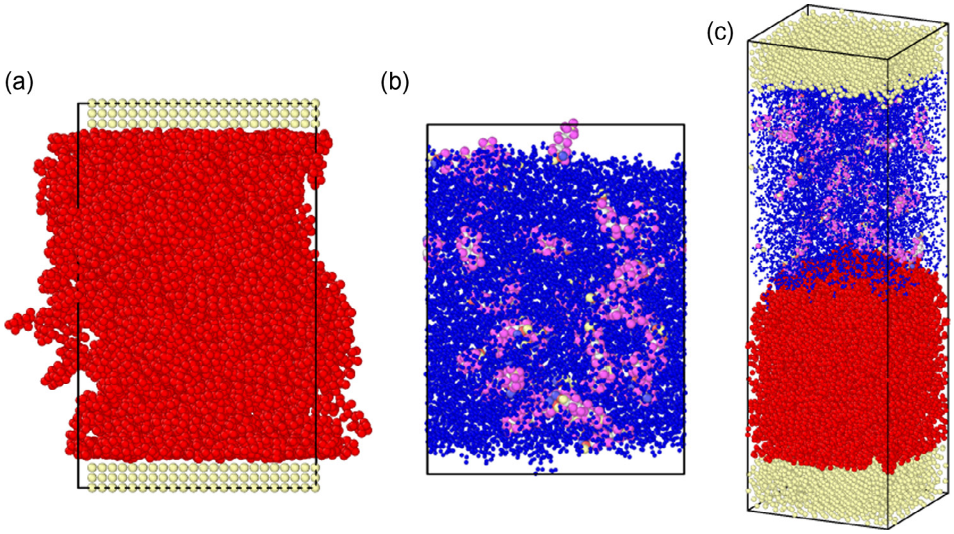

Fig. 5. The atomistic C8-water-polymer layer system at 300 K; (a) the polymer film layer; (b) the C8 and the water layer, and (c) the assembled diffusion layer model. The yellow, the red and the blue colors represent, respectively, the rigid walls, the polymer film, and the water molecules. (For interpretation of the references to colour in this figure legend, the reader is referred to the web version of this article.)

During the simulations, the diffusion of C8 molecules into the polymer matrix is characterized by the self-diffusion coefficient D_s. Using the mixture systems shown in Fig. 4, D_s is computed by using

$$D_s = \frac{\sum_{i=1}^{N} D_i}{N} \tag{4}$$

where N is the number of C8 molecules in the polymer matrix, and D_i the self-diffusion coefficient of the single C8 molecule i in the polymer matrix calculated by using the following Einstein relation:

$$D_i = \lim_{t\to\infty} \frac{\langle (r^i_{com}(t) - r^i_{com}(0))^2 \rangle}{6t} \tag{5}$$

where $\langle (r^i_{com}(t) - r^i_{com}(0))^2 \rangle$ represents the mean-square displacement (MSD) of the C8 molecule i and t is the simulation time.

Since the diffusion of small molecules is known to be concentration- and temperature- dependent, thus for studying the concentration effects, we have investigated the diffusion of 20, 30, 60, 90 and 120 C8 molecules in the polymer film systems that, respectively, equal the concentration of 1.7%, 2.5%, 5%, 7.5%

and 10%. For analyzing the temperature effects, we have investigated the temperature range of 300–360 K, which is within the temperature bound for storing C8-related food products.

3. Results and discussions

3.1. CG model verification

In Section 2.2, we described the development of the CG models for each polymer component. Though the same MARTINI modeling framework is used for each constituent, its transferability to describe the C8-polymer system with the mixed polymer components should be further examined. Accordingly, the mass densities and the structure properties of the simulated binary systems are first checked.

In Table 5 we have summarized the mass densities of the atomistic and the CG C8-polymer systems after the NVT-NPT equilibrium cycles. The CG densities are found to match reasonably well with the atomistic densities for the five C8 concentrations studied. For the atomistic simulations, the system's overall mass density slightly decreases with an increase of the C8 concentration. This can be explained from the swelling effects of the added C8 molecules in the polymer matrix that increases the volume. However, the situation is opposite for the CG simulations since an increase in the number of C8 molecules results in a small increase of the overall mass density. This indicates that the swelling effects of C8 molecules are weak in the CG systems, which can be attributed to the simpler and softer non-bonded interactions (e.g., no Coulombic interactions) used in the CG models. Considering that the largest difference in mass densities of the atomistic and the corresponding CG models is only about 3.0% (for the highest C8 concentration), we conclude that the developed CG parameters based on the individual polymer component are suitable to describe the mass density of the mixed C8-polymer system.

The local structural features of the atomistic and the CG binary systems are also checked. The inter-molecular radial pair distribution function, (r), is used to characterize the structure properties for the C8-polymer interactions and the interactions among various polymer segments. In Fig. 6, we have exhibited the C8-polymer $g(r)$ results for systems with 1.7% and 10% C8 concentrations. The $g(r)$ is calculated between the P1 bead in C8 molecules and the SC2, Na and SP3 beads in the PMA/EAA chains. The $g(r)$ results of atomistic simulations are obtained by transferring the atomistic trajectories into the CG trajectories. From results displayed in Fig. 6, it can be seen that the distribution heights of the atomistic and the CG $g(r)$ are different for the three pairs, the corresponding distance values (abscissa in Fig. 6) that reflect the non-bonded interactions are quite close to each other. The P1-SP3 and the P1-Na pairs are observed to be more structured than the P1-SC2 pair for both the atomistic and the CG $g(r)$ which indicates that the C8 molecules tend to interact more with the SP3 and the Na side segments of the EAA and the PMA chains in the polymer matrix. The values listed in Table 3 suggest that the P1-SP3 and the P1-Na pairs indeed have a stronger interaction strength than the P1-SC2 pair. Besides the interaction strength, the relatively more free spaces provided by the branching side segments of the polymer chains also contribute to the P1-SP3 and the P1-Na interactions [21]. In Fig. 7 we have exhibited the $g(r)$ distribution between various polymer chains, including PMA-PMA, EAA-EAA and PMA-EAA pairs, for systems with 1.7% and 10% C8 concentrations. It can be seen that the PMA-PMA and the EAA-EAA pairs exhibit two peaks in $g(r)$ distributions (Fig. 7a and b). The first peak represents the intramolecular bonded interactions, while the second peak is related to the non-bonded interactions (either intramolecular or intermolecular). For the bonded interactions, the $g(r)$ of the CG models match well with those of the atomistic models, regardless of the C8 concentration. This is expected since the CG parameters are directly developed by reproducing the bond and the angle distributions. For the non-bonded interactions, the $g(r)$ distributions in CG models show a small deviation from that in the atomistic models. They slightly increase with an increase in the C8 concentration. The corresponding pair distances also show that the PMA (or the EAA) chains in the CG models have a slightly larger separation distance from each other than those in the atomistic models. Though the non-bonded $g(r)$ distributions for the PMA-PMA and the EAA-EAA pairs between CG and atomistic models do not perfectly match with each other, there is a much better matching for the PMA-EAA case (Fig. 7d). For the PMA-EAA pair, the $g(r)$ distributions are also observed to decrease with an increase in the C8 concentration, which may be due to the swelling induced by adding more C8 molecules in the matrix. Considering that the CG non-bonded parameters are determined by using the MARTINI force field's definitions, it is encouraging to see from these $g(r)$ distributions that with these "simple" parameters, the local structure features of the polymer matrix are reasonably well reproduced by the developed CG models.

The multiple peaks (multimodal distribution) in the P1-P1 radial pair distribution functions in Fig. 7b are not sufficient to imply that the C8 molecules are clustering in the system. We further checked the equilibrated microstructure of the 120 C8-polymer system (see Fig. 7d). It can be seen that the 120 C8 molecules are uniformly dispersed in the polymer matrix rather than clustered into several groups. The multimodal distribution seen in Fig. 7b is due to the uniformly distributed C8 molecules in the current cases. The distributions of C8 molecules in the polymer matrix are important during their diffusions, thus, the P1-P1 pairs are also analyzed for the two systems with 1.7% and 10% C8 concentrations. Comparing the atomistic and the CG P1-P1 distributions shown in Fig. 8, we see that the two distribution heights and the two corresponding distances agree well with each other. This means that the atomistic and the CG models have similar starting points for the diffusion of C8 molecules. For systems with low C8 concentration (Fig. 8a), both the atomistic and the CG distributions are unimodal indicating the dispersion feature of the C8 molecules in the polymer matrix after their equilibration (see Fig. 4). For systems with high C8 concentration (Fig. 8b), even though the P1-P1 distributions exhibit a multimodal mode, a closer examination of the equilibrated microstructure (not shown)

Table 5
Mass densities and self-diffusion rates of C8 molecules for various concentrations in atomistic and CG C8-polymer systems at 300 K.

Number of C8	Atomistic density ρ^{AA} (g cm^{-3})	Self-diffusion rate D_s^{AA} ($\times 10^{-11}$ m^2 s^{-1})	CG density ρ^{CG} (g cm^{-3})	Self-diffusion rate D_s^{CG} ($\times 10^{-11}$ m^2 s^{-1})	Scaling factor D_s^{CG}/D_s^{AA}
20	0.925 ± 0.005	0.203	0.937 ± 0.004	0.589	2.901
30	0.925 ± 0.005	0.398	0.937 ± 0.005	0.983	2.470
60	0.922 ± 0.006	0.452	0.940 ± 0.004	1.498	3.313
90	0.920 ± 0.005	0.621	0.943 ± 0.004	1.896	3.053
120	0.918 ± 0.005	0.943	0.945 ± 0.005	1.989	2.089

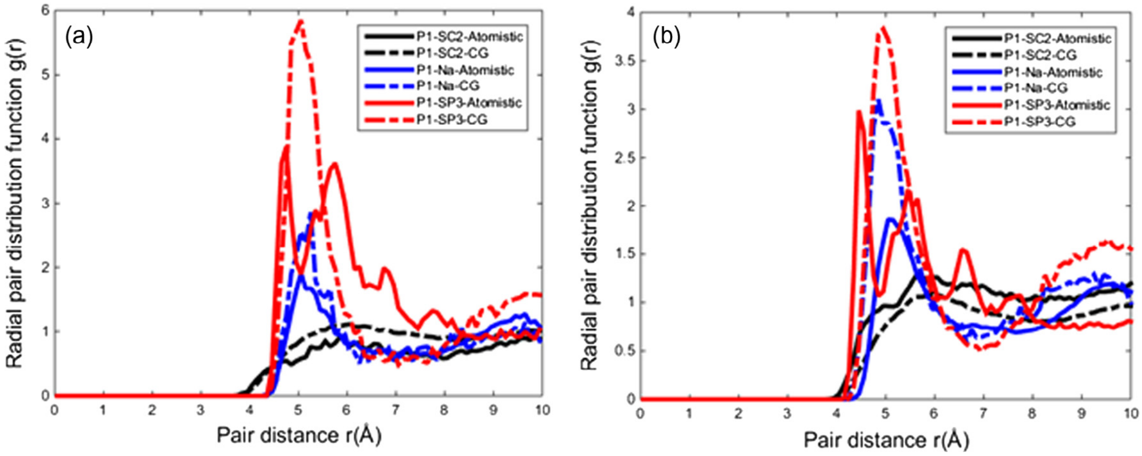

Fig. 6. Radial pair distribution functions between the C8 molecules and the PMA/EAA polymer chains for the atomistic and the CG binary systems for (a) 1.7% C8 and (b) 10% C8 concentration. (For interpretation of the references to colour in this figure legend, the reader is referred to the web version of this article.)

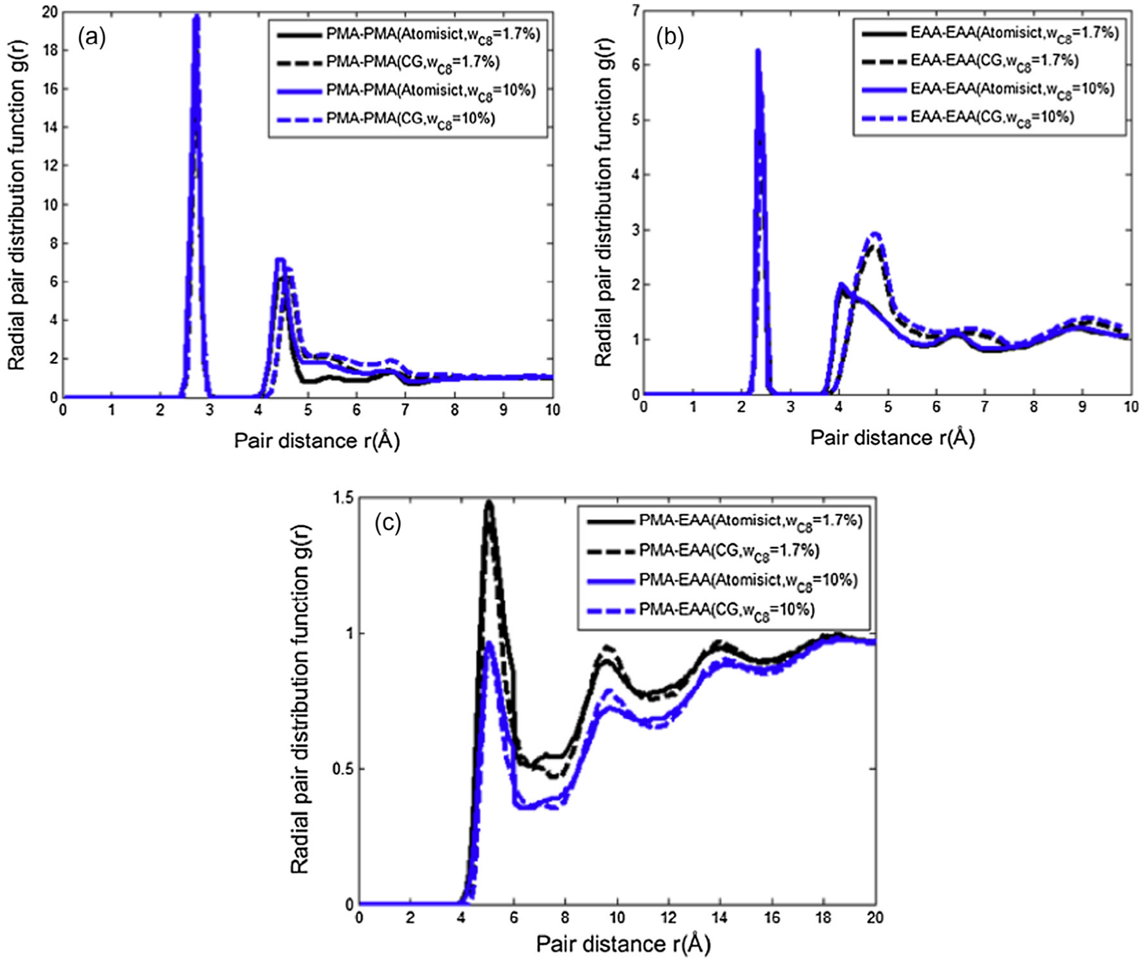

Fig. 7a–c. Radial pair distribution functions between polymer chains for the atomistic and the CG binary systems (with 1.7% and 10% C8 concentrations), (a) PMA-PMA, (b) EAA-EAA, and (c) PMA-EAA. (For interpretation of the references to colour in this figure legend, the reader is referred to the web version of this article.)

confirms that the C8 molecules are still uniformly dispersed in the polymer matrix, rather than clustered into groups. Since all these structural features (e.g., C8-polymer, polymer-polymer and C8-C8 structures) between the atomistic and the CG models match well, we conclude that the developed CG parameters are suitable for describing the studied binary systems and the diffusions of C8 molecules.

3.2. Diffusion of C8 molecules

The main goals of the present work are to (i) develop a CG modeling framework for evaluating the barrier properties of a complex polymeric film for the penetrators, and (ii) test the developed CG framework as an analysis tool to guide the design of polymeric films with a tailored barrier property for the penetrators. In

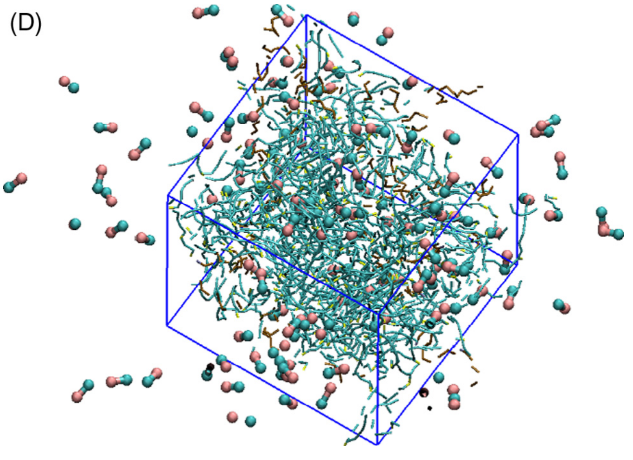

Fig. 7d. CG model of the equilibrated 120 C8-polymer system at 300 K. (For interpretation of the references to colour in this figure legend, the reader is referred to the web version of this article.)

experiments, the barrier property of the polymeric film is usually characterized by the penetration coefficient, $P = D_m \cdot S$ (where D_m is the mutual-diffusion coefficient and S the solubility coefficient). Through a thermodynamic correction (e.g., the Darken equation), the mutual-diffusion coefficient, D_m, can be related to the self-diffusion coefficient, D_s, of the penetrator molecules in the polymer matrix. Therefore, in the current work, we focused on examining the ability of the developed CG models to predict the ensemble-averaged self-diffusion coefficients D_s^{CG} and their scaling factors to map D_s^{CG} to the physical time scale in atomistic simulations. These scaled D_s^{CG} then will serve as the reference values for estimating the barrier properties of a complex polymer film.

We note that by using the present CG models and parameters, we have computed the D_m^{CG} for the barrier property of the polymeric film by simulating the CG small molecule-polymer film inter-diffusion [36]. The time scaling factors determined in the current work is used to calibrate the measured D_m^{CG} to D_m in real physical time.

The above-developed CG models well reproduce the local structure features of C8-polymer system. Therefore, their ability to describe the dynamic behaviors and the self-diffusion coefficients D_s of the C8 molecules into the polymer matrix are studied in this section.

Given the equilibrated C8-polymer systems shown in Fig. 4, the D_s of C8 molecules can be obtained by monitoring their COM trajectories and the corresponding mean-square displacements (MSDs) during the simulations. In Fig. 9 and Table 5 we have summarized the calculated D_s values from the two simulation approaches at 300 K. Within the studied concentration range, the diffusion rates D_s^{CG} obtained from the CG simulations are higher than those calculated from the atomistic simulations, D_s^{AA}. These higher D_s^{CG} values are due to the larger beads and the smoother potentials used in the CG simulations, which significantly weaken the friction effects present in the atomistic simulations. Both diffusion constants D_s^{AA} and D_s^{CG} are observed to increase with the increase of C8 concentration. This indicates that the developed CG models capture the well-known concentration-dependent diffusion behaviors of small molecules in the polymer matrix, which is due to the swelling effect of additive small molecules in the polymer matrix. A closer examination of the histories of the dynamic behavior of C8 molecules (Fig. 9b) reveals that the CG models also capture the two diffusion mechanisms, hopping and trapping [16,18], for small molecules diffusion into the polymer matrix. It means that though the smoother potentials are used in the developed CG models, they do not alter the diffusion mechanisms for the C8 molecules.

Even though the CG simulations have an intrinsic time unit based on which the D_s^{CG} values are calculated, it does not necessarily represent the physical time scale for the simulated systems [28,35]. In order to interpret the D_s^{CG} results in the CG simulations, we need to calibrate the time scale for the CG models. Marrink et al. [28] proposed that as a first approximation one can simply scale the time axis for the dynamic phenomena with the atomistic models. They found that the effective time scale for the MARTINI force field is about 2–10 times larger than that of the atomistic models with the exact value depending upon the mapping rule. A coarser mapping scheme that has a smaller friction in the CG description would result in a larger factor for the dynamics phenomena. In the current CG simulations, the diffusion coefficients D_s^{CG} obtained from the MSD history is directly scaled with D_s^{AA} to interpret the effective time for the diffusion of C8 molecules. The results are summarized in Table 5. It is found that the scaling factors are around 2–3 times larger for all CG models with different C8 concentrations which is consistent with the employed finer (2-to-1 and 3-to-1) mapping schemes in Section 2.2. Though the D_s^{AA} is used as the scaling target for the CG models, it is noted that only relatively short MD runs of the CG dynamics are required to reach

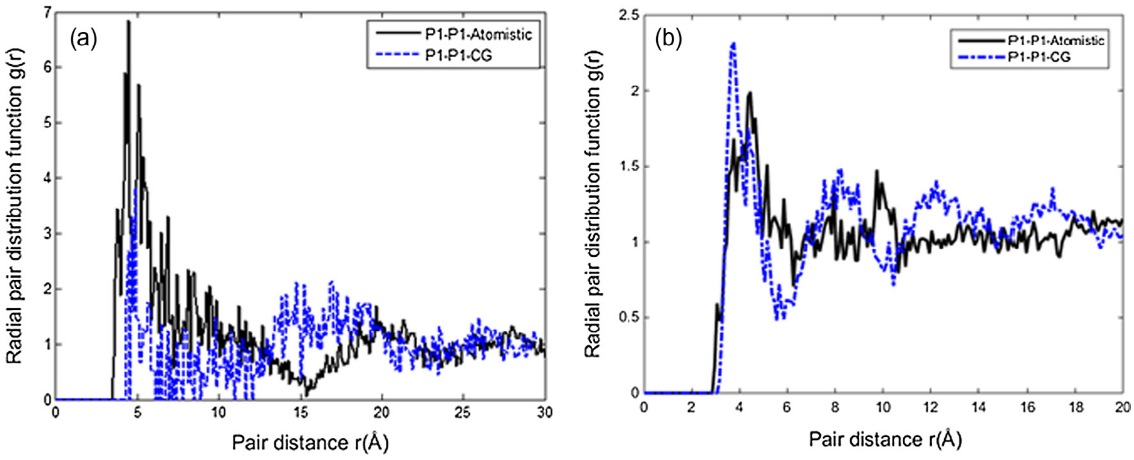

Fig. 8. Radial pair distribution functions between C8 molecules for the atomistic and the CG binary systems with (a) 1.7% C8 and (b) 10% C8 concentration. (For interpretation of the references to colour in this figure legend, the reader is referred to the web version of this article.)

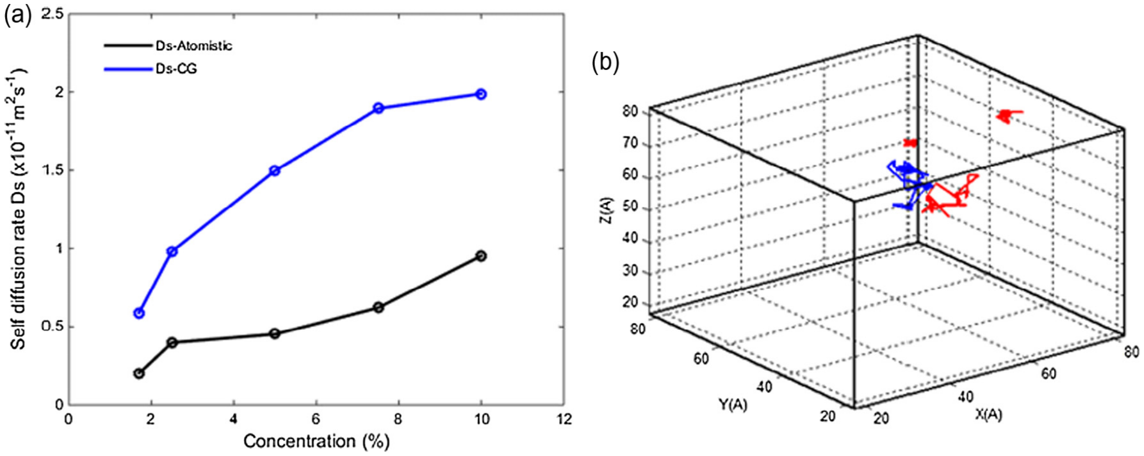

Fig. 9. (a) Concentration-dependent D_s of the C8 molecules in the polymeric film; (b) Trajectories of four selected CG C8 molecules in the 1.7% concentration system. Two dynamic modes, hopping and trapping, can be observed. (For interpretation of the references to colour in this figure legend, the reader is referred to the web version of this article.)

the normal diffusive regime. However, for the atomistic simulations, at least one order of magnitude more simulation time is needed to obtain reasonably accurate values of the diffusion constants. Thus, based on the calibrated time scaling factors, the developed CG simulation method can be applied to more efficiently study the diffusion of small molecules into the polymer matrix for the evaluation of the polymer's barrier property. That is, the D_s^{CG} values derived from the CG simulation results can be used to estimate the D_s^{AA}, which are usually calculated on a time scale that is too long for the direct atomistic simulations. Then, based on the interpreted D_s^{CG} values, the barrier property of the polymer film for the small molecules can be preliminarily estimated.

3.3. Temperature dependence of diffusion coefficients

In order to assess the transferability of the above identified time scale factors, we performed both atomistic and CG simulations in the temperature range of 300–360 K by using the models with 1.7% C8 concentration. The results for the dependence of the diffusion constants of C8 molecules upon the temperature are reported in Table 6. It is found that both D_s^{AA} and D_s^{CG} values increase as the temperature increases which is due to the higher mobility of C8 molecules and the polymer chains. Scaling the D_s^{CG} with D_s^{AA}, it is encouraging to see that the time scaling factors for the CG models are also around 2–3 times for the studied temperature range. This indicates that the CG parameters developed at T = 300 K are transferable to higher temperatures. It is also noted from values listed in Table 6 that the mass densities of both the atomistic and the CG models are lower at the higher temperature. However, due to the larger density reduction, the corresponding thermal expansion rate is found to be higher for the atomistic model. The different thermal expansion rate may affect the time scaling between the atomistic and the CG models through the generation of various free volumes for the C8 diffusion. However, by examining the activation barrier energy for the C8 diffusion using the Arrhenius equation, it is found that the activation energy for the atomistic and the CG models are 48.2 kJ/mol and 45 kJ/mol, respectively. This indicates that within the studied temperature range, the different thermal expansion rate in the atomistic and the CG models has negligible effects on the C8 diffusion and the corresponding time scale factor.

We note that our goal is not to develop the CG framework with a temperature-transferable potential. Rather, we are more interested in examining the temperature range for which the developed CG parameters can be transferred. This is why we test the stability of the scaling factor from 300 K to 360 K since a relatively stable scaling factor (within that temperature range) will allow us to better estimate the diffusion coefficients from CG models. As the temperature is further increased ($\gg$360 K), a temperature-dependent scaling factor is expected.

3.4. Effect of the presence of water

The diffusion of C8 molecules into a barrier polymeric film usually occurs in an aqueous environment, such as that in a canned food [37]. In order to check the extension of the proposed multiscale method for this scenario, the effect of the presence of water on the C8 diffusion is studied by using the atomistic and the CG layer models. Figs. 10 and 11 show the microstructure evolutions for the two C8-water-polymer systems. The C8 molecule, water and polymer chains are represented by purple, blue and red colors, respectively. In Fig. 10, we see that the C8 molecules are evenly distributed in the water layer at the beginning of the diffusion. They gradually are absorbed onto the polymer surface due to their low solubility in water (560 mg/L at 25 °C) and strong binding affinity to the polymeric film (109 kJ/mol at 26.85 °C) [38]. Accom-

Table 6
Mass densities and self-diffusion rates of C8 molecules at different temperatures found using the atomistic and the CG C8-polymer systems at 1.7% C8 concentration.

T (K)	Atomistic density ρ^{AA} (g cm^{-3})	Self-diffusion rate D_s^{AA} ($\times10^{-11}$ m^2 s^{-1})	CG density ρ^{CG} (g cm^{-3})	Self-diffusion rate D_s^{CG} ($\times10^{-11}$ m^2 s^{-1})	Scaling factor D_s^{CG}/D_s^{AA}
300	0.925 ± 0.005	0.203	0.937 ± 0.004	0.589	2.901
320	0.917 ± 0.008	0.725	0.930 ± 0.005	1.786	2.461
330	0.902 ± 0.010	1.220	0.929 ± 0.006	3.337	2.734
340	0.905 ± 0.010	2.642	0.929 ± 0.006	6.201	2.347
350	0.899 ± 0.012	3.076	0.923 ± 0.008	6.630	2.156
360	0.891 ± 0.012	4.952	0.921 ± 0.008	12.37	2.569

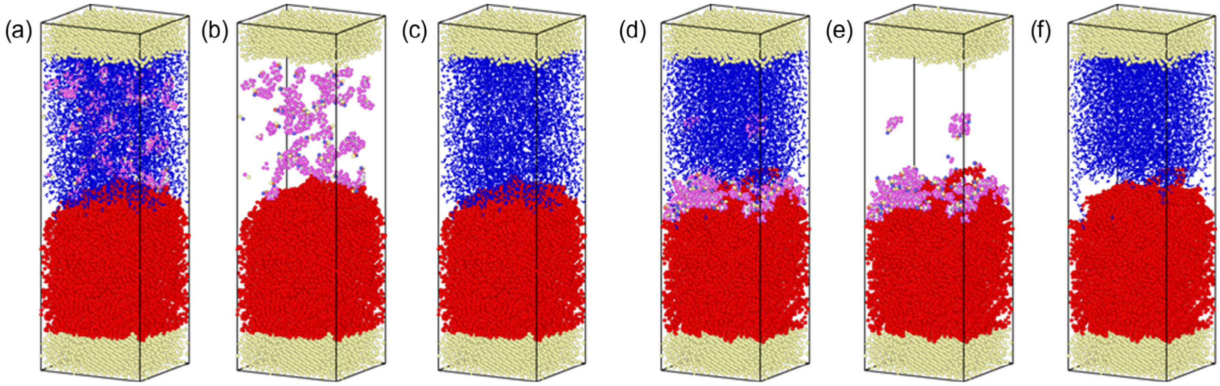

Fig. 10. Microstructure evolutions of C8-water-polymer atomistic layer system at (a)–(c) t = 0 ns, and (d)-(f) t = 5 ns. The yellow, red and blue colors represent, respectively, rigid walls, the polymer film, and the water molecules. The water molecules in (b) and (e), and the C8 molecules in (c) and (f) are not shown for clearly viewing. (For interpretation of the references to colour in this figure legend, the reader is referred to the web version of this article.)

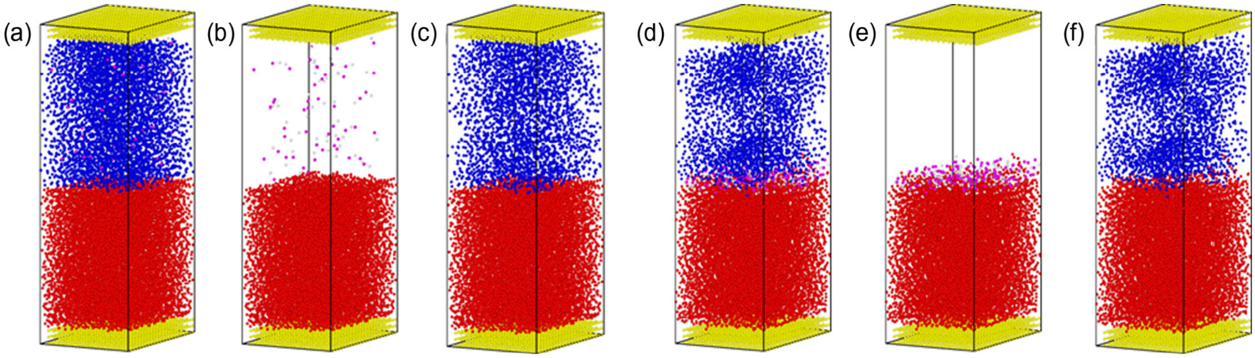

Fig. 11. Microstructure evolutions of C8-water-polymer CG layer system at (a)-(c) t = 0 ns and (d)–(f) t = 10 ns. The yellow, red and blue colors represent, respectively, rigid walls, the polymer film, and the water molecules. The water molecules in (b) and (e), and the C8 molecules in (c) and (f) are not shown for clearly viewing. (For interpretation of the references to colour in this figure legend, the reader is referred to the web version of this article.)

panying with the C8 adsorption, water molecules are drained away from the polymer surface and only a few of them (<5) are observed to penetrate into the polymer film. This is consistent with the water resistance nature of EAA polymers that make 40%wt of the film. After the adsorption, the C8 molecules start to diffuse into the polymer chains, which is driven by the chemical potential and the concentration gradient. The above observed C8 adsorption and water resistance phenomena depicted in Fig. 10 can also be clearly seen from results exhibited in Fig. 11 which indicate that the developed CG model not only well captures the dynamic behavior of C8 molecules in the aqueous environment, but also the water solubility of the polymer matrix. Since the diffusion of absorbed C8 molecule into the polymer film in the atomistic model (Fig. 10) is extremely slow, it makes the developed CG model a very desirable alternative method to accelerate the diffusion [36].

To quantitatively compare the dynamic behaviors of the C8 and water molecules in both atomistic and CG systems, their MSDs are monitored during the simulations. Fig. 12 shows the MSDs results and the corresponding time-dependent self-diffusion coefficients. From the MSDs, it is seen that the water molecules diffuse faster than the larger C8 molecules in both atomistic and CG systems. We note that in the MARTINI force field, each CG water bead represents the center-of-mass of four real water molecules. The average MSD of the center-of-mass of four molecules is theoretically 4 times less than the average MSD of the four individually diffusing molecules [27]. Thus, a slower MSD of the water molecules (about 3.5 times) is observed in the CG system in Fig. 12a. In contrast, since each CG C8 molecule represents exactly one real C8 molecule, therefore, they are observed to diffuse faster (about 1.9 times) in the CG model than in the atomistic model due to the coarse graining. The above average MSDs only tell the overall dynamics behavior of the C8 and water molecules. To describe the adsorption behaviors of C8 molecules onto the polymer surface, the time-dependent self-diffusion coefficients are calculated and shown in Fig. 12b. It is seen that the C8 self-diffusion coefficients gradually decrease with time for both atomistic and CG models. This can be understood from the reduced mobility of C8 molecules due to the constraining effects from the polymer chains after their absorption. It is expected that after all the adsorbed C8 molecules diffuse into the polymeric film, the C8 self-diffusion rates will reach a steady state [36]. Due to the same adsorption mechanisms, an identical C8 diffusion rate reduction is observed for the two systems in Fig. 13b. This indicates the capability of the developed CG models to describe the C8 diffusion in the aqueous environment.

3.5. Effect of the polymer component weight percentage

The developed CG models are parameterized based on each polymer component in the film, which makes a potential CG method useful for studying the polymer systems with same components but different weight percentage to guide the polymeric film design. To access this feature of the developed CG models, we simulated the diffusion of 20 C8 molecules in five polymer systems at T = 300 K and T = 360 K with 20, 40, 60, 80 and 100 PMA chains, respectively. In these polymeric film systems, the chain numbers of the remaining three components are kept the same as 87 EAA, 5 BPEI and 5 LPEI. The calculated C8 self-diffusion rates,

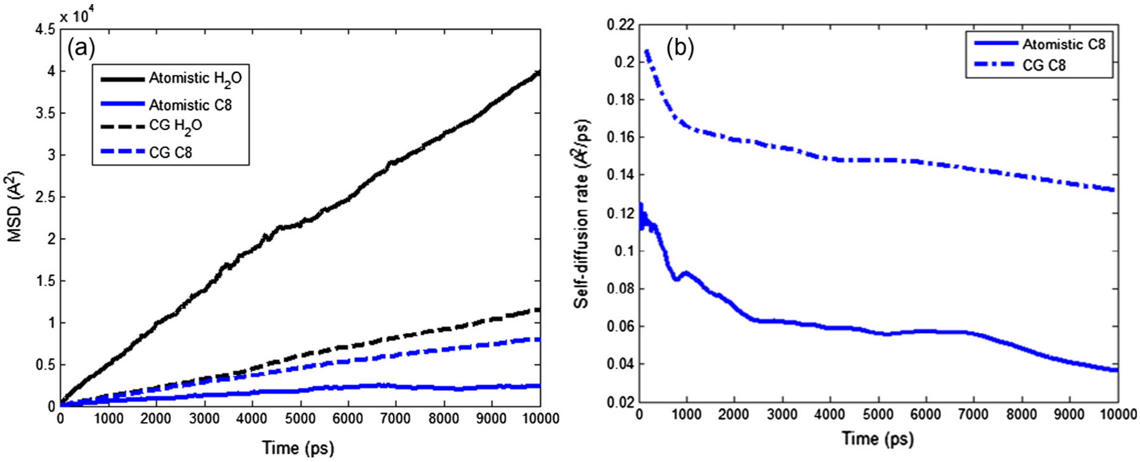

Fig. 12. Time histories of (a) the mean-square displacements (MSDs) and (b) the self-diffusion coefficients of the C8 and water molecules for C8-water-polymer atomistic and CG layer systems. (For interpretation of the references to colour in this figure legend, the reader is referred to the web version of this article.)

which are the averaged five measurements for each C8-polymer system, are summarized in Table 7 and shown in Fig. 13. It is seen that the mass density of the systems and the corresponding diffusion rates of C8 molecules, increase with the addition of more PMA chains into the system at T = 300 K and T = 360 K. For both atomistic and CG systems, the mass density (ρ^{AA} and ρ^{CG}) increases by about 10% after adding additional 80 PMA chains (e.g., at T = 300 K, ρ^{AA} and ρ^{CG} increase, respectively, from 0.925 g cm^{-3} and 0.937 g cm^{-3} to 1.022 g cm^{-3} and 1.049 g cm^{-3}; at T = 360 K, ρ^{AA} and ρ^{CG} increase from 0.891 g cm^{-3} and 0.921 g cm^{-3} to 0.984 g cm^{-3} and 1.012 g cm^{-3}, respectively), making it more close to the mass density of pure PMA polymer (1.22 g cm^{-3}). Accompanying with the increase in the mass density, the D_s^{C8} also increases for both the atomistic and the CG systems. This can be understood from the branching chemical structure of the PMA chains (see Fig. 2a) which provides additional free spaces for the diffusion of C8 molecules when more PMA chains are added into the film. Examining the scaling factors between the CG and atomistic models, it is seen that they are in the range of 2–3, indicating the feasibility of applying the developed CG methods to the design of the polymeric barrier film.

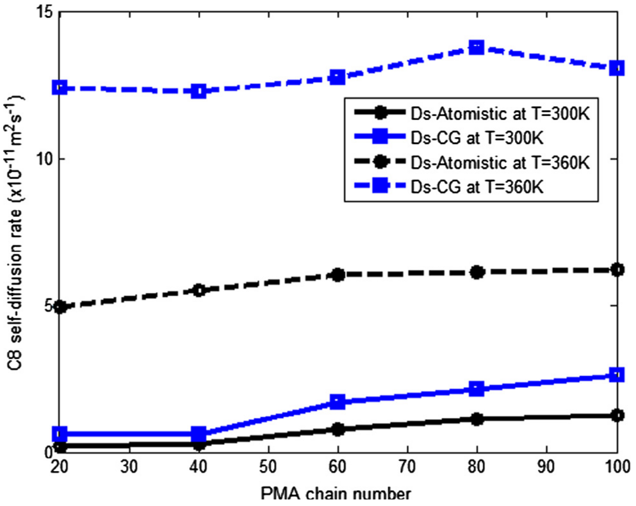

Fig. 13. Self-diffusion rates of 20 C8 molecules in polymer films with different PMA chain number at T = 300 K and T = 360 K. (For interpretation of the references to colour in this figure legend, the reader is referred to the web version of this article.)

3.6. Discussion of results

The MARTINI force field is employed in the current CG modeling. Even though there are four different components in the studied polymer matrix, the CG parameterization is independently identified for each component. When the CG bead types for each component are determined (e.g., Na-SC2 beads for the PMA polymer, SC2-SP3 beads for the EAA polymer, etc.), their non-bonded interactions (Table 3) are also determined according to the conventional definitions in the MARTINI force field. Thus, our CG parameterization focuses mainly on the bonded interactions that are based on the atomistic distance and the angle distributions for each component. If the atomistic distance and the angle distributions are unimodal, then the corresponding CG parameters can be uniquely identified. However, it is noted that the atomistic

Table 7
Self-diffusion rates of C8 molecules in polymer films with different weight percentage of PMA found using the atomistic and the CG C8-polymer systems at 1.7% C8 concentration.

T (K)	PMA number	Atomistic density ρ^{AA} (g cm^{-3})	Self-diffusion rate D_s^{AA} ($\times 10^{-11}$ m^2 s^{-1})	CG density ρ^{CG} (g cm^{-3})	Self-diffusion rate D_s^{CG} ($\times 10^{-11}$ m^2 s^{-1})	Scaling factor D_s^{CG}/D_s^{AA}
300	20	0.925 ± 0.005	0.203	0.937 ± 0.004	0.589	2.901
	40	0.958 ± 0.005	0.398	0.975 ± 0.005	0.614	2.020
	60	0.983 ± 0.006	0.452	1.005 ± 0.004	1.679	2.186
	80	1.001 ± 0.006	0.621	1.028 ± 0.005	2.128	1.890
	100	1.022 ± 0.006	0.943	1.049 ± 0.005	2.621	2.129
360	20	0.891 ± 0.012	4.952	0.921 ± 0.008	12.37	2.498
	40	0.922 ± 0.012	5.517	0.946 ± 0.008	12.27	2.224
	60	0.947 ± 0.012	6.033	0.974 ± 0.008	12.72	2.108
	80	0.971 ± 0.012	6.121	1.003 ± 0.008	13.73	2.243
	100	0.984 ± 0.012	6.201	1.012 ± 0.009	13.07	2.108

distance and the angle distributions are always bimodal or multimodal (see Fig. 3 for the EAA polymer) which is due to the choice of the mapping scheme and the non-tacticity of the polymer chains. The CG parameters are adjusted to produce distributions that cover as many atomistic distribution areas as possible. Using this distribution area mapping rule, even though the identified CG parameters are not necessarily unique (e.g., the bond/angle strengths can vary within a small range), they can still well reproduce structural characteristics (e.g., the radius of gyration) of the polymer components for the subsequent diffusion analysis. Based on the distribution area mapping rule, an optimal algorithm can be applied to the CG parameterization process to obtain the "unique" optimal parameter sets for each polymer component.

Due to the use of coarser particles and smoother interaction potentials, the local barriers of polymer chains for C8 diffusion in the CG model are not the same as those in the atomistic model. As compared to the atomistic models, the CG models overestimate the diffusion of solute molecules into the polymeric film and the corresponding activation barriers for penetration motion are lower. The Arrhenius equation can be used to estimate the activation barrier energy for the diffusion in both CG and atomistic models:

$$D_s = D_0 \exp\left(-\frac{E_a}{RT}\right) \tag{6}$$

Here D_0 is the pre-exponential factor, E_a the activation energy, R the ideal gas constant and T the absolute temperature. Using the temperature-dependent values of D_s in Table 6, the calculated activation energies are 45 kJ/mol and 48.2 kJ/mol for the CG and the atomistic models, respectively. The smaller activation energy for diffusion in the CG model can be qualitatively understood from the reduced local friction in the system, which then results in a higher C8 mobility (or diffusion). The reduced (smaller) barriers for the C8 diffusion is an inherent feature of current CG models, since the smoother bonded interactions are used and the non-bonded interactions (especially those between the C8 and the polymer beads) are directly inherited from the MARTINI force field definition (e.g., all interaction distances are set equal to either 0.47 nm or 0.43 nm). This issue can be alleviated if a more rigorous CG parameterization procedure (for both bonded and non-bonded interactions) can be developed to map the free energy profiles of all those interactions. With the rigorous procedure, the barriers for diffusion will be accurately represented. The high efficiency of the CG models is due to the reduced number of degrees of freedom. However, for the current CG modeling of the C8-polymer system, the presence of four components (EAA, PMA, BPEI and LPEI polymers) in the polymer matrix makes it very challenging to apply the above-mentioned rigorous CG parameterization method, since it is very difficult to obtain the exact free energy profiles for all interactions among beads in the system. Thus, one has to compromise. In the current work, since we are more interested in obtaining the ensemble-averaged self-diffusion coefficients, the smoother non-bonded interaction potentials inherited from the MARTINI force field are used in the simulations. We expect qualitatively the same diffusion mechanism (hopping and trapping) for the CG C8 molecules in the CG polymer matrix as for the atomistic system (see Fig. 8a). The use of the MARTINI force field facilitates modeling of the complex polymer matrix with four constituents.

The developed CG models for studying the diffusion of C8 molecules into a polymeric film greatly extends the accessible timescale. This CG time-scale is often interpreted by comparing the chain self-diffusion coefficient D_s^{CG} to values from the atomistic simulations D_s^{AA}. From the comparison of results listed in Tables 5 and 6, it is found that the concentration and the temperature effects scale well between the CG and the atomistic models with a scaling ratio of 2–3. It indicates that the developed CG parameters have a relatively good quality of concentration and temperature transferability, though they are determined under the particular thermodynamic state at T = 300 K. This is a desirable property, which means, within the studied concentration and temperature ranges, a CG simulation spanning 1 microsecond would correspond to 2–3 μs in real time for our model.

We note that the CG model cannot predict accurate values of the diffusion coefficients especially when the scaling factor is concentration- and temperature-dependent. However, the scaling factor is inevitable for most CG modeling works reported in the literature because the intrinsic time in the CG model is not necessarily the physical time for the dynamics of the systems. Thus, one needs to carefully interpret/determine the time scaling factor in using CG simulations for a quantitative analysis of time-dependent phenomena. Because length scales are fixed by the CG bead mapping procedure from the very beginning, thus one can identify the time scaling factor by mapping the MSDs of the CG simulations onto the data from the atomistic simulations (or by comparing the self-diffusion coefficients, D_s^{CG}/D_s^{AA}). For the penetrator-polymer systems, given the penetrator concentration and the simulation temperatures higher than polymer's Tg, a "fixed" time scaling factor can be expected. Using this "fixed" time scaling factor, we were able to estimate the system's dynamic properties through CG models. In the current study of C8-polymer CG systems, the time scaling factors are determined to be between 2 and 3 for the investigated concentration and temperature ranges. Thus, when interpreting the CG model simulation results one can, to a first approximation, simply use the factor 3 (or 2) to obtain the diffusion coefficients.

The cross-linking has not been considered in the polymer matrix. However, it will not significantly affect the observed concentration and temperature effects on the time scaling relation between the CG and the atomistic models, especially at high temperatures because the diffusion of C8 molecules is mainly affected by local motions of the surrounding EAA and the PMA segments and there is no cross-linking between these segments. Thus, according to the Einstein relation, the C8 molecules diffusion coefficient (both in the atomistic and the CG models) is defined as:

$$D_{c8} \approx \frac{kT}{N\xi} \tag{7}$$

where ξ is the friction coefficient, N the number of local atoms/beads, k the Boltzmann constant and T the absolute temperature. At a high temperature (>T_g) when continuum diffusion dominates, the cross-linking will not greatly alter $N\xi$, therefore, it will not significantly affect the scaling relationship $\tau = D_{C8}^{CG}/D_{C8}^{AA}$. However, at a low temperature ($\ll T_g$), the above Einstein relation is not valid since the C8 molecules are trapped in the polymer matrix which makes it difficult to find the effective friction coefficient and the accurate value of the diffusion coefficient thereby making the scaling relationship $\tau = D_{C8}^{CG}/D_{C8}^{AA}$ unreliable.

For the current uncross-linked CG model, T_g is about 315 K [36]. Thus, according to the Einstein relation, the temperature (300–360 K) and the concentration (300 K) effects would scale well between the CG and the atomistic models. When the cross-linking is considered, the T_g will increase making it difficult to obtain accurate values of D_{C8}^{AA} and D_{C8}^{CG} at temperatures $\ll T_g$ and hence the scaling relationship.

The degree of the coarse-graining rather than the cross-linking will significantly affect the time scaling relationship between the CG and the atomistic models. This can be understood from the value of $N\xi$ in Eq. (7), which is inversely proportional to the diffusivity D_{c8}^{CG}. The coarser the CG polymer mapping, the smaller the value of $N\xi$ for the C8 molecules and thus a larger value of the time scaling factors would be obtained. Another factor that may also influence the time scaling is the chemical proprieties of the molecules themselves in the diffusion systems. For example, the hydrogen bonding, which cannot be easily incorporated in the CG models, has been reported to make the atomistic dynamics at low temperatures much slower than the CG counterparts [39]. For the current simulated systems, no hydrogen bonds form between the C8 molecules and the polymer chains. Therefore, a relatively stable time scaling relationship between the CG and the atomistic models is observed.

As shown in Fig. 9b, the diffusion mechanisms of C8 molecules into the polymer matrix are trapping and hopping (for both atomistic and CG systems). Therefore, it is expected that the local motions of surrounding EAA and PMA segments will significantly affect movements of C8 molecules and the subsequent diffusion coefficient calculation based on the MSDs. It is thus inferred that due to the limited number of cross-linking sites in the system (the PMA and the EAA chains are cross-linked through the BPEI and the LPEI chains), the C8 molecules will have a similar local surrounding environment when compared with the cross-linked system. Therefore, introducing the cross-linking in the system will not essentially alter the calculated concentration- and temperature-dependent self-diffusion coefficients, and then the corresponding time scale factors. However, we should note that though the cross-linking has a minor effect on the self-diffusion calculation in the mixture systems, it will greatly influence the C8-polymer interdiffusion into the layered systems.

4. Conclusions

We have developed a multiscale method that combines the atomistic and the MARTINI force field-based CG simulations to study the diffusion of small molecules into an uncross-linked polymer matrix. The atomistic simulations are used to parameterize the CG parameters and calibrate the CG time scales. The faster CG simulations are used to explore the dynamics of small molecules in larger systems and for longer times. As an example problem, the developed method is applied to analyze the diffusion of C8 molecules into a commercial polymeric film composed of four constituents, and delineate effects of the concentration, the temperature and water on the diffusion of C8 molecules. The conclusions of this study are summarized below.

(1) Even though the CG parameters are developed for the specific polymer components studied here, the mass density and the local structure analysis results indicate that they are suitable for describing the diffusion of small additives into a polymeric matrix since the same MARTINI force field modeling framework can be used in the parameterization process.
(2) The developed CG method captures the concentration- and the temperature-dependent diffusion behaviors of C8 molecules into the polymeric film. For the studied concentration and temperature ranges, the time scaling factor between the CG and the atomistic models varies between 2 and 3 that agrees well with the mapping schemes employed.
(3) The developed CG parameters well reflect the water resistance properties of the polymer matrix, which allows the CG model to capture the diffusion of C8 molecules into the polymeric film in an aqueous environment.
(4) The developed CG model is capable of predicting the self-diffusion rates of C8 molecules in the polymeric films of different weight percentage of PMA components. This feature is useful in designing a polymeric film with a tailored barrier property.

Acknowledgements

Authors are grateful to the two anonymous reviewers whose comments on the manuscript have considerably helped improve upon the presentation of the work.

References

[1] J. Crank, The mathematics of diffusion, Clarendon Press, Oxford [England], 1975.
[2] J.S. Vrentas, J.L. Duda, J. Polym. Sci.: Polym. Phys. Ed. 15 (3) (1977) 403–416.
[3] J.S. Vrentas, C.M. Vrentas, Eur. Polym. J. 34 (5–6) (1998) 797–803.
[4] E. von Meerwall, S. Beckman, J. Jang, W.L. Mattice, J. Chem. Phys. 108 (10) (1998) 4299–4304.
[5] S.A. Stern, H.L. Frisch, Annu. Rev. Mater. Sci. 11 (1) (1981) 523–550.
[6] S.A. Stern, V. Saxena, J. Membr. Sci. 7 (1) (1980) 47–59.
[7] A.T. DiBenedetto, D.R. Paul, J. Polym. Sci. Part A: Gen. Pap. 2 (2) (1964) 1001–1015.
[8] R.J. Pace, A. Datyner, J. Polym. Sci.: Polym. Phys. Ed. 17 (3) (1979) 437–451.
[9] S.B. Kulkarni, M.Y. Kariduraganavar, T.M. Aminabhavi, J. Appl. Polym. Sci. 89 (12) (2003) 3201–3209.
[10] R. Gavara, R. Catalá, P.M. Hernández-Muñoz, R.J. Hernández, Packag. Technol. Sci. 9 (4) (1996) 215–224.
[11] D. Cava, J.M. Lagarón, A. López-Rubio, R. Catalá, R. Gavara, Polym. Test. 23 (5) (2004) 551–557.
[12] R.A. Waggoner, F.D. Blum, J.M.D. MacElroy, Macromolecules 26 (25) (1993) 6841–6848.
[13] P.T. DeLassus, Sorption and Diffusion of Flavors in Plastic Packaging, in: Flavor-Food Interactions, vol. 633, American Chemical Society, 1996, pp. 152–161.
[14] M. Kobayashi, T. Kanno, K. Hanada, S.-I. Osanai, J. Food Sci. 60 (1) (1995) 205–209.
[15] R. Franz, Packag. Technol. Sci. 6 (2) (1993) 91–102.
[16] G.E. Karlsson, T.S. Johansson, U.W. Gedde, M.S. Hedenqvist, Macromolecules 35 (19) (2002) 7453–7459.
[17] Z.-W. Wang, P.-L. Wang, C.-Y. Hu, Packag. Technol. Sci. 23 (8) (2010) 457–469.
[18] S. Neyertz, D. Brown, Macromolecules 41 (7) (2008) 2711–2721.
[19] A.E. Ismail, F. Pierce, G.S. Grest, Mol. Phys. 109 (16) (2011) 2025–2033.
[20] S.G. Charati, S.A. Stern, Macromolecules 31 (16) (1998) 5529–5535.
[21] A. Mattozzi, M.S. Hedenqvist, U.W. Gedde, Polymer 48 (17) (2007) 5174–5180.
[22] A. Gautieri, S. Vesentini, A. Redaelli, J. Mol. Model. 16 (12) (2010) 1845–1851.
[23] G. Milano, F. Müller-Plathe, J. Phys. Chem. B 109 (39) (2005) 18609–18619.
[24] Q. Sun, R. Faller, Comput. Chem. Eng. 29 (11–12) (2005) 2380–2385.
[25] W. Shinoda, R. DeVane, M.L. Klein, Mol. Simul. 33 (1–2) (2007) 27–36.
[26] S.O. Nielsen, C.F. Lopez, G. Srinivas, M.L. Klein, J. Chem. Phys. 119 (14) (2003) 7043–7049.
[27] S.J. Marrink, A.H. de Vries, A.E. Mark, J. Phys. Chem. B 108 (2) (2004) 750–760.
[28] S.J. Marrink, H.J. Risselada, S. Yefimov, D.P. Tieleman, A.H. de Vries, J. Phys. Chem. B 111 (27) (2007) 7812–7824.
[29] H. Lee, A.H. de Vries, S.-J. Marrink, R.W. Pastor, J. Phys. Chem. B 113 (40) (2009) 13186–13194.
[30] P. Nikunen, I. Vattulainen, M. Karttunen, Phys. Rev. E 75 (3) (2007) 036713.
[31] W.L. Jorgensen, J. Chandrasekhar, J.D. Madura, R.W. Impey, M.L. Klein, J. Chem. Phys. 79 (2) (1983) 926–935.
[32] W.L. Jorgensen, D.S. Maxwell, J. Tirado-Rives, J. Am. Chem. Soc. 118 (45) (1996) 11225–11236.
[33] R.W. Hockney, J.W. Eastwood, Computer Simulation using Particles, CRC Press, 1988.
[34] S. Plimpton, J. Comput. Phys. 117 (1) (1995) 1–19.
[35] V.A. Harmandaris, N.P. Adhikari, N.F.A. van der Vegt, K. Kremer, B.A. Mann, R. Voelkel, H. Weiss, C. Liew, Macromolecules 40 (19) (2007) 7026–7035.
[36] E. Lin, X. You, R.M. Kriegel, R.D. Moffitt, R.C. Batra, Polymer 115 (2017) 273–284.
[37] M.G. Sajilata, K. Savitha, R.S. Singhal, V.R. Kanetkar, Compreh. Rev. Food Science and Food Safety 6 (1) (2007) 17–35.
[38] E. Lin, X. You, R.M. Kriegel, R.D. Moffitt, R.C. Batra, Colloids Surf., A 522 (2017) 152–160.
[39] P. Carbone, H.A.K. Varzaneh, X. Chen, F. Müller-Plathe, J. Chem. Phys. 128 (6) (2008) 064904.